This Accepted Manuscript has not been copyedited and formatted. The final version may differ from this version. A link to any extended data will be provided when the final version is posted online.

JNeurosci
THE JOURNAL OF NEUROSCIENCE

Research Articles: Cellular/Molecular

Resilience to Pain: A Peripheral Component Identified using induced Pluripotent Stem Cells and Dynamic Clamp

Malgorzata A. Mis[1,2], Yang Yang[1,2], Brian S. Tanaka[1,2], Carolina Gomis-Perez[1,2], Shujun Liu[1,2], Fadia Dib-Hajj[1,2], Talia Adi[1,2], Rolando Garcia-Milian[3], Betsy R. Schulman[1,2], Sulayman D. Dib-Hajj[1,2] and Stephen G. Waxman[1,2]

[1]*Department of Neurology; Yale University, New Haven, CT*

[2]*Center for Neuroscience & Regeneration Research, VA Connecticut Healthcare System, West Haven, CT*

[3]*Bioinformatics Support Program, Cushing/Whitney Medical Library, Yale University, New Haven, CT*

https://doi.org/10.1523/JNEUROSCI.2433-18.2018

Received: 20 September 2018

Revised: 29 October 2018

Accepted: 7 November 2018

Published: 20 November 2018

Author contributions: M.M., Y.Y., S.D.D.-H., and S.G.W. designed research; M.M., Y.Y., B.S.T., C.G.-P., S.L., F.d.-h., T.A., and B.R.S. performed research; M.M., Y.Y., C.G.-P., R.G.-M., S.D.D.-H., and S.G.W. analyzed data; M.M., Y.Y., and S.G.W. wrote the first draft of the paper; S.D.D.-H. and S.G.W. wrote the paper.

Conflict of Interest: The authors declare no competing financial interests.

Funding: This work was supported by Center Grant B9253-C from the U.S. Department of Veterans Affairs Rehabilitation Research and Development Service, by a grant from The Erythromelalgia Association, and by the Regenerative Medicine Research Fund (RMRF) of CT Innovations. The Center for Neuroscience and Regeneration Research is a Collaboration of the Paralyzed Veterans of America with Yale University. Author contributions: M.A.M., Y.Y., S.D.D.-H., and S.G.W. designed research; Y.Y., M.A.M., B.S.T., C.G.-P, S.L., F.D-F., T.A., R.G-M. and B.R.S. performed research; M.A.M., Y.Y., S.D.D.-H. and S.G.W. analyzed data; M.A.M., Y.Y., S.D.D.-H., and S.G.W. wrote the paper. Data and materials availability: Whole Exome Sequencing data are available through the dbGaP (accession # phs001724.v1.p1). We thank Palak Shah, Dr. Mark Estacion, Dr. Sameet Mehta and Christopher Castaldi for technical support.

Correspondence should be addressed to To whom correspondence should be addressed: Stephen G. Waxman, MD/PhD; Neuroscience and Regeneration Research Center, VA Connecticut Healthcare System, 950 Campbell Avenue, Bldg. 34, West Haven, CT 06516, Tel: (203) 937-3802, Fax: (203) 937-3801, E-mail: stephen.waxman@yale.edu

Cite as: J. Neurosci 2018; 10.1523/JNEUROSCI.2433-18.2018

Alerts: Sign up at www.jneurosci.org/alerts to receive customized email alerts when the fully formatted version of this article is published.

Accepted manuscripts are peer-reviewed but have not been through the copyediting, formatting, or proofreading process.

Copyright © 2018 the authors

JNeurosci Accepted Manuscript

JNeurosci Accepted Manuscript

1 **Resilience to Pain: A Peripheral Component Identified using induced**
2 **Pluripotent Stem Cells and Dynamic Clamp**
3
4 **Abbreviated title:** Modeling differences in pain profiles using iPSCs.

5 Malgorzata A. Mis[1,2#], Yang Yang[1,2#], Brian S. Tanaka[1,2], Carolina Gomis-Perez[1,2],
6 Shujun Liu[1,2], Fadia Dib-Hajj[1,2], Talia Adi[1,2], Rolando Garcia-Milian[3], Betsy R.
7 Schulman[1,2], Sulayman D. Dib-Hajj[1,2], and Stephen G. Waxman[1,2*]
8
9 [1]Department of Neurology; Yale University, New Haven, CT, 06510.
10 [2]Center for Neuroscience & Regeneration Research, VA Connecticut Healthcare
11 System, West Haven, CT, 06516.
12 [3]Bioinformatics Support Program, Cushing/Whitney Medical Library, Yale University,
13 New Haven, CT, 06510.
14 # these authors contributed equally
15 ***To whom correspondence should be addressed:** Stephen G. Waxman, MD/PhD;
16 Neuroscience and Regeneration Research Center, VA Connecticut Healthcare System,
17 950 Campbell Avenue, Bldg. 34, West Haven, CT 06516, Tel: (203) 937-3802, Fax:
18 (203) 937-3801, E-mail: stephen.waxman@yale.edu

19 **Number of pages:** 38
20 **Number of figures:** 5 + 3 extended data figures
21 **Words for Abstract:** 237
22 **Words for Introduction:** 631
23 **Words for Discussion:** 1126
24 **Conflict of interest:** The authors declare no competing financial interests.
25

JNeurosci Accepted Manuscript

26 **Acknowledgments:**

27 **Funding:** This work was supported by Center Grant B9253-C from the U.S. Department
28 of Veterans Affairs Rehabilitation Research and Development Service, by a grant from
29 The Erythromelalgia Association, and by the Regenerative Medicine Research Fund
30 (RMRF) of CT Innovations. The Center for Neuroscience and Regeneration Research is
31 a Collaboration of the Paralyzed Veterans of America with Yale University. **Author**
32 **contributions:** M.A.M., Y.Y., S.D.D.-H., and S.G.W. designed research; Y.Y., M.A.M.,
33 B.S.T., C.G.-P, S.L., F.D-F., T.A., R.G-M. and B.R.S. performed research; M.A.M., Y.Y.,
34 S.D.D.-H. and S.G.W. analyzed data; M.A.M., Y.Y., S.D.D.-H., and S.G.W. wrote the
35 paper. **Data and materials availability:** Whole Exome Sequencing data are available
36 through the dbGaP (accession # phs001724.v1.p1**)**.
37 We thank Palak Shah, Dr. Mark Estacion, Dr. Sameet Mehta and Christopher Castaldi
38 for technical support.

39

40
41
42
43
44
45
46
47
48
49
50
51

JNeurosci Accepted Manuscript

52 **Abstract:**

53

54 Pain is a complex process that involves both detection in the peripheral nervous system
55 and perception in the central nervous system. Individual-to-individual differences in pain
56 are well-documented, but not well-understood. Here we capitalized on inherited
57 erythromelalgia (IEM), a well-characterized human genetic model of chronic pain, and
58 studied a unique family containing related IEM subjects with the same disease-causing
59 Nav1.7 mutation, which is known to make dorsal root ganglion (DRG) neurons
60 hyperexcitable, but different pain profiles (affected son with severe pain, affected
61 mother with moderate pain and an unaffected father). We show, first, that at least in
62 some cases, relative sensitivity to pain can be modeled in subject-specific iPSC-derived
63 sensory neurons *in vitro*; second, that in some cases, mechanisms operating in
64 peripheral sensory neurons contribute to inter-individual differences in pain; and third,
65 using Whole Exome Sequencing (WES) and dynamic clamp we show that it is possible
66 to pinpoint a specific variant of another gene, *KCNQ* in this particular kindred, that
67 modulates the excitability of iPSC-derived sensory neurons in this family. While different
68 gene variants may modulate DRG neuron excitability and thereby contribute to inter-
69 individual differences in pain in other families, this study shows that subject-specific
70 iPSCs can be used to model inter-individual differences in pain. We further provide
71 proof-of-principle that iPSCs, WES, and dynamic clamp can be used to investigate
72 peripheral mechanisms and pinpoint specific gene variants that modulate pain signaling
73 and contribute to inter-individual differences in pain.

74

75

JNeurosci Accepted Manuscript

76 **Significance**

77 Individual-to-individual differences in pain are well-documented, but not well-
78 understood. In this study we show, first, that at least in some cases, relative sensitivity
79 to pain can be modeled in subject-specific iPSC-derived sensory neurons *in vitro*;
80 second, that in some cases, mechanisms operating in peripheral sensory neurons
81 contribute to inter-individual differences in pain; and third, using Whole Exome
82 Sequencing (WES) and dynamic clamp we show that it is possible to pinpoint a specific
83 gene variant that modulates pain signaling and contributes to inter-individual differences
84 in pain.

85

86 **Introduction**

87 Chronic pain affects more than 250 million individuals worldwide, and the lack of
88 effective pain treatment has contributed to the opioid crisis. Inter-individual differences
89 in pain are well-documented, with some individuals reporting more severe pain, and
90 others reporting less severe pain in response to similar noxious insults. However,
91 individual-to-individual variation in pain has not been accurately modeled in the
92 laboratory and its mechanistic basis remains incompletely understood, partially because
93 pain involves both detection in the peripheral nervous system and perception in the
94 central nervous system, and involves processes that operate at multiple levels including
95 genetic, epigenetic, environmental and social.

96 Inherited erythromelalgia (IEM) is an autosomal dominant disorder characterized
97 by episodes of intense burning pain in the distal extremities in response to mild warmth
98 that provides a human genetic model of chronic pain with a well-defined causative

JNeurosci Accepted Manuscript

99 molecular substrate (Drenth and Waxman, 2007). IEM is caused by gain-of-function
100 mutations in voltage-gated sodium channel $Na_V1.7$, which is mainly expressed in the
101 peripheral nervous system, that produce hyperexcitability in peripheral sensory (dorsal
102 root ganglion; DRG) neurons. More than a dozen $Na_V1.7$ channel mutations have been
103 reported to cause IEM via this mechanism (Dib-Hajj et al., 2013). Interestingly, even for
104 patients carrying the same $Na_V1.7$ mutation, differences in pain have been documented
105 (Geha et al., 2016; McDonnell et al., 2016). Little is known about the cellular or
106 molecular basis for differences in pain in patients with the same $Na_V1.7$ mutation and
107 thus far, the difference in pain has not been modeled at the bench.

108 We have capitalized on IEM as a well-characterized genetic model of chronic
109 pain, and studied a unique kindred containing two IEM subjects from the same family
110 (mother and son), both carrying the $Na_V1.7$-S241T mutation, which is known to enhance
111 channel activation (Lampert et al., 2006) and produce hyperexcitability of DRG neurons
112 (Yang et al., 2012). The son displayed a much more severe pain profile (higher number
113 and longer duration of attacks, and higher number of nightly awakenings) compared to
114 his mother (Geha et al., 2016). We used subject-specific induced pluripotent stem cells
115 (iPSCs) to ask whether the individual-to-individual difference in pain profiles might be
116 modeled in a “disease-in-a-dish” model (McNeish et al., 2015) in the laboratory and
117 studied this phenomenon at the cellular and molecular levels. We asked whether the
118 difference in pain between these two individuals might, at least in part, be a result of
119 different firing properties of their peripheral sensory neurons, and further, asked whether
120 we could identify molecular contributors to the differences in these pain profiles.

JNeurosci Accepted Manuscript

121 Cells derived from iPSCs retain the genetic background and native transcriptional
122 machinery of affected patients (Inoue et al., 2014; Zeltner and Studer, 2015; Soliman et
123 al., 2017). We prepared iPSCs from blood samples of the affected son (P300; severe
124 pain) and mother (P301; mild pain) carrying the $Na_V1.7$-S241T mutation, and from an
125 unaffected family member (P303, P300's father) and differentiated these iPSCs into
126 peripheral sensory neurons (iPSC-SNs) for disease modeling. We demonstrate that
127 iPSC-SNs derived from these subjects display significant differences in firing frequency
128 and spontaneous activity that parallel their different pain profiles. Using whole exome
129 sequencing (WES), we discovered multiple gene variants that might contribute to
130 neuronal excitability and that might serve as modifiers of sensory neuron firing. We then
131 identified a variant of one particular gene (*KCNQ* in this kindred) as a contributor to
132 differences in pain between these two individuals. While different gene variants may
133 affect DRG neuron excitability and thereby contribute to inter-individual differences in
134 pain in other families, this study shows that it is possible to model inter-individual
135 differences in pain using subject-specific iPSCs. We further provide proof-of-concept
136 that WES and dynamic clamp can be used to investigate peripheral mechanisms and
137 pinpoint specific gene variants that modulate pain signaling and contribute to inter-
138 individual differences in pain.
139
140
141
142
143

JNeurosci Accepted Manuscript

144 **Materials and Methods**

145 **Generation of induced pluripotent stem cells (iPSCs)**

146 iPSCs were generated from the blood samples of two IEM subjects (mother (P301) and
147 son (P300) carrying Nav1.7-S241T mutation) and an unaffected individual (father
148 (P303)) using CytoTune-iPS 2.0 Sendai Reprogramming Kit (ThermoFisher Scientific)
149 according to the manufacturer protocol. Cells were screened for pluripotent stem cell
150 markers and tested for normal karyotype. iPSCs were cultured for at least 10
151 generations before the start of differentiation into sensory neurons (iPSC-SNs). The
152 study was approved by the Yale Human Investigation Committee.

153 **Differentiation of iPSC into sensory neurons**

154 Differentiation was initiated using a modified Chambers protocol using LSB and 3i
155 inhibitors (Chambers et al., 2012; Young et al., 2014; Cao et al., 2016). Differentiated
156 neurons were maintained in Neurobasal medium supplemented with N2/B27 GlutaMAX
157 (ThermoFisher Scientific) and nerve growth factors: Recombinant Human ßNGF, brain-
158 derived neurotrophic factor (BDNF), glial cell line–derived neurotrophic factor (GDNF),
159 neurotrophin-3 (NT-3) (25 µg/ml; PeproTech) for 8 weeks before functional assessment.

160 **Immunocytochemistry**

161 iPSC-SNs were immunostained with markers for sensory neurons. Primary antibodies
162 were incubated overnight at 4°C in PBS-T (0.1% TritonX100,2%BSA, 4% Donkey
163 serum in PBS; Pan Neuronal Marker-Alexa488 conjugate, 1:100, MAB2300X - Millipore;
164 Peripherin 1:200, SC-7604 - Santa Cruz; BRN3A, 1:200, AB5945 - Millipore; Nav1.7,
165 1:250, Y083; Islet 1, 1:200 ab86501, Abcam). Secondary antibodies were incubated for

JNeurosci Accepted Manuscript

166 2h at room temperature in PBS-T. Images were acquired using a Nikon C1 confocal
167 microscope (Nikon).

168 **Multi Electrode Array Recordings**

169 Multi Electrode Array (MEA) experiments were carried out with a multi-well MEA system
170 (Maestro, Axion Biosystems) according to our recently developed protocol (Yang et al.,
171 2016). Briefly, iPSC-SNs were dissociated and cultured on MEA plates, maintained at
172 37ºC in a 5% CO_2 incubator. A 12-well recording plate was used, embedded with a total
173 of 768 electrodes. For each experiment, three wells (with ~192 available electrodes for
174 recording) were used to assess iPSC-SNs derived from P301 (mother), P300 (son) and
175 P303 (father).

176 **Whole-cell current-clamp electrophysiology**

177 Whole-cell current-clamp recordings were obtained for head-to-head comparisons from
178 iPSC-SNs from paired differentiations prepared contemporaneously and processed in
179 parallel by the same technician and studied by the same electrophysiologist.
180 Recordings were amplified using an Axon MultiClamp 700B amplifier. Data were
181 digitized via an analogue to digital converter Digidata 1440a and stored on a personal
182 computer using pClamp 10.4 software, which was also used to define and execute
183 protocols. The data were filtered at 5 kHz and acquired at 50 kHz. Electrodes used for
184 the recordings had resistance of < 1.5 MΩ when filled with the internal solution, which
185 consisted of (mM): KCl 140; HEPES, 5; EGTA, 0.5; Mg-ATP, 3; Dextrose 20; pH 7.3,
186 295-300 mOsm. iPSC-SNs were continuously perfused with external recording solution
187 containing (mM): NaCl, 140; KCl, 3; HEPES-NaOH, 10; MgCl2, 2; CaCl2, 2; Dextrose,
188 15; pH 7.3, ~320 mOsm.

JNeurosci Accepted Manuscript

189 **Whole exome sequencing and analysis**

190 Whole exome sequencing (WES) was performed at Yale Center for Genome Analysis
191 following a previously published protocol (Zaidi et al., 2013; Jin et al., 2017). Three
192 subjects were included for sequencing analysis: proband carrying Nav1.7-S241T
193 mutation, proband's mother carrying Nav1.7-S241T mutation, and proband's unaffected
194 father. The obtained reads were filtered and trimmed for quality and aligned to the hg19
195 version of the human genome (GRCh37) using aligner (BWA-MEM). From the aligned
196 reads, we used variant caller (GATK) to call the variants from each sample. We
197 extracted the significant variants based on genotyping quality score and coverage of the
198 reference and alternative base (the criteria are at least 3 reads with alternative base,
199 and at least 20% of coverage is alternative base). All the variants that passed the filter
200 were then collected across all the samples using custom-built python scripts.

201 Ensembl's Variant Effect Predictor (VEP) was used to determine the effect of the
202 resulting variants and Ingenuity Pathway Analysis (IPA, Build 470319M Version
203 43605602, Qiagen) was used to carry out functional annotation analyses for gene
204 ontology functions analyses (http://www.ingenuity.com/).

205 **RT-PCR and sequencing**

206 RNA was isolated from iPSC-SNs from P300, P301 and P303 using RNeasy plus kit
207 (Qiagen Cat#74134) according to the manufacturer's protocol. RNA concentration was
208 measured on a Nanodrop, and total RNA (100 ng) was used to generate cDNA using
209 Bio-Rad iScript Reverse Transcription Supermix (Cat#170-8841). One ml cDNA was
210 used as a template for PCR amplification in a final volume of 50 ml. High Fidelity,
211 AccuPrime Taq DNA Polymerase (ThermoFisher Cat#12346-086) was used for

JNeurosci Accepted Manuscript

212 amplification. At least one of the primers crosses an exon-intron boundary to distinguish
213 cDNA products from potential genomic DNA contamination.

214 Thermal cycling was initiated at 94°C for 2 minutes followed by 35 cycles of 30 s at
215 94°C, annealing for 30 s at 55°C for Nav1.7 (60°C for Kv7.2), and an extension for 60 s
216 at 68°C. Because of high GC content, PCR was performed with 6% DMSO for Kv7.2.
217 The following primers were used: 5'-ATCACGGACAAGGACCGCACC-3' and 5'-
218 TCCTGCCGCAGGAACTCCATG-3' generating a 512 bp fragment for Kv7.2; 5'-
219 TGCAAGAGGCTTCTGTGTAGG-3' and 5'- GCTCGTGTAGCCATAATCAGG-3'
220 generating a 514 bp fragment for Nav1.7. The identity of the amplicon was verified by
221 Sanger sequencing using the purified PCR product (PCR clean-up, Gel extraction kit,
222 Macherey-Nagel Cat# 740609.50), and the same forward and reverse primers that were
223 used for PCR amplification. Sequencing was done at the Keck DNA Sequencing facility
224 at Yale University.

225 **Perforated-patch I_M recordings in iPSC-SNs**

226 Recordings were obtained using EPC-10 amplifier and the PatchMaster program (HEKA
227 Elecktronik). Data were sampled at 4 kHz and filtered at 2.9 kHz low-pass Bessel filter.
228 Patch pipette resistance was 2-3 MΩ and series resistance was compensated (60-
229 90%).

230 Extracellular bath solution contained the following (mM): 144 NaCl, 2.5 KCl, 2 $CaCl_2$,
231 0.5 MgCl, 5 HEPES, and 10 Glucose, pH adjusted to 7.4 with NaOH. The bath was
232 supplemented with 5 mM 4-aminopyridine (4-AP) to block the fast-activating Kv1
233 channels, 1 µM Tetrodotoxin (TTX) to inhibit sodium currents and 20 µM 4-
234 ethylphenylamino-1,2-dimethyl-6-methylaminopyrimidinium chloride (ZD-7288) to block

JNeurosci Accepted Manuscript

235 hyperpolarization-activated cyclic nucleotide (HCN)-gated currents. Pipettes were filled
236 with an intracellular solution containing (mM): 80 K-acetate, 30 KCl, 40 HEPES, 3 MgCl,
237 3 EGTA and 1 $CaCl_2$, pH adjusted to 7.4 with NaOH. Liquid junction potential (LJP) was
238 corrected (+8.2 mV). All the recordings were performed at room temperature. Data were
239 analyzed using Fitmaster (HEKA, Elektronik) and Origin (Microcal Software).
240 iPSC-SNs were recorded in the perforated patch configuration using Amphotericin B to
241 reduce run-down, a stock solution of 1 mg/20 µl DMSO was prepared and stored in the
242 dark. For recordings, 2 µl of the stock were dissolved in 1 ml of intracellular solution
243 using an ultrasonicator. Fresh batch of solution was remade every 2 hours.
244 M-current (I_M) was identified by using a standard deactivation voltage protocol (Adams
245 and Brown, 1982), in which cells are held at -20 mV, to activate the current and then
246 deactivated by intermittent hyperpolarizing steps.
247 The I-V curves were calculated according to Adams et al (Adams et al.,
248 1982). We measured the instantaneous current I(Vh) and the steady-state current, the
249 total current measured after the slow relaxation is complete Iss(V); the intersection of
250 these two currents give the reversal potential and under our conditions the reversal
251 potential was -78.2 mV, close to the calculated E_K. Leak obtained by extrapolation of the
252 linear portion of the I-V curve between -100 to -70 was then subtracted according to
253 Passmore et al (Passmore et al., 2003). The I_M (leak-subtracted-steady state) currents
254 were normalized and plotted vs membrane voltages.
255 The conductance of I_M was assessed according to Adams et al. The current
256 values (I_M) were divided by the driving force and normalized to the maximal value to
257 obtain the conductance (gKv7/M); $\Delta G_M = \Delta I_M(V)/(V-Vm)$ (Adams and Brown, 1982;

JNeurosci Accepted Manuscript

258 Adams et al., 1982). Data were fitted with a Boltzmann curve: g/gmax = A1 – A2 (1 +
259 exp (v – v1/2)/ Kl) -1, where V1/2 is the half-maximal activation voltage, A1 and A2 are
260 the minimum and maximum values and Kl is the curve slope. Liquid junction potential
261 (LJP) was corrected (+8.2 mV).

262 **Dynamic clamp recordings**

263 iPSC-SNs were dynamically clamped in whole-cell configuration (Petrovic et al., 2012;
264 Battefeld et al., 2014; Vasylyev et al., 2014) to introduce model I_M conductance based
265 on the kinetic model of I_M. The extracellular and pipette solutions had the same
266 composition as those used for current clamp recordings. Electrode resistance was ~
267 1MΩ when filled with the intracellular solution. Membrane voltages and currents were
268 recorded in dynamic clamp with a MultiClamp 700B amplifier (Molecular Devices)
269 interfaced with CED Power 1401 mkII DAI and Signal 6 software (CED), digitized by
270 Digidata 1440A DAC, and stored on hard disk for off-line analysis using pCLAMP 10.6
271 software (Molecular Devices). Recordings were performed at room temperature.

272 **Kinetic model of I_M-current**

273 The gating variable for I_M is described using a Hodgkin-Huxley differential equation
274 $dn/dt = \alpha_n(1 - n) - \beta_n n$, where n is the channel activation variable and α(β) is forward
275 (reverse) rate constants, respectively. I_M steady-state parameters and kinetics obtained
276 from electrophysiological recordings were converted into rate constants at respective
277 voltages using the equations $\alpha = n/\tau$, $\beta = (1 - n)/\tau$. Liquid junction potentials (+8.2 mV)
278 were adjusted for all parameters. Reaction rate constants were fitted with a Boltzmann
279 equation and converted into steady-state activation variable and time constant
280 according to $n = \alpha/(\alpha + \beta)$ and $\tau = 1/(\alpha + \beta)$. WT and T730A I_M models were calculated in

JNeurosci Accepted Manuscript

281 a 28-pF equipotential sphere of 1 μF/cm^2 capacitance with a conductance density of
282 0.00014 S/cm2.
283 The following rate constants were used for P300 (homozygous KCNQ2-WT)
284 Kv7.2 channel model:
285 $\alpha_n = 0.00594/(1 + \exp(-(V + 60.28)/6.40))$,
286 $\beta_n = 0.015/(1 + \exp(V + 57.82)/20.38)$
287 P301 Kv7.2 channel (heterozygous WT/ T730A) was described by the following rate
288 constant:
289 $\alpha_n = 0.00541/(1 + \exp(-(V + 72.80)/11.08))$,
290 $\beta_n = 0.014/(1 + \exp(V + 72.71)/11.63)$
291 I_M conductance was modelled using Hodgkin-Huxley formalism as a non-
292 inactivating current described by $I_M = g_M * n (V – E_K)$, where g_M is the maximal
293 conductance, n represents an activation gate, E_K is the potassium reversal potential,
294 and V is the membrane potential. Currents evoked by different voltage protocols were
295 calculated in 10-μs precision with a custom program written in OriginPro 8.5 LabTalk.
296
297 **Experimental design and statistical analysis**
298 *MEA*
299 To minimize potential variations during the recordings, iPSC-SNs from all three subjects
300 were differentiated on the same day with same reagents. iPSC-SNs were always plated
301 on MEA plates by the same investigator. A spike detection criterion of >6 standard
302 deviations above background signals was used to separate monophasic and biphasic
303 action potential spikes from noise. We defined active electrodes as registering >1

JNeurosci Accepted Manuscript

304 recorded spike over a 200 s period (Yang et al., 2016). MEA data were analyzed using
305 Axion Integrated Studio AxIS2.1 (Axion Biosystems) and NeuroExplorer (Nex
306 Technologies) (Yang et al., 2017).

307 To assess the firing properties under different temperatures, the precise
308 temperature control of the MEA system was utilized, which enables continuous
309 monitoring of neuronal firing during temperature ramps. iPSC-SNs from P301, P300 and
310 P303 were plated on the same MEA plate for the temperature ramp study, and
311 assessed by an investigator blinded to the genotype. Three different temperatures
312 (33ºC, 37ºC and 40ºC) were used during the study, and each temperature was
313 maintained for 7-10 min to allow analysis of steady-state neuronal firing at each
314 condition.

315 *Whole-cell current-clamp*

316 Only iPSC-SNs with stable membrane potential were chosen for analysis. Resting
317 membrane potential was determined immediately after switching into current-clamp
318 mode as the mean membrane voltage in the absence of current stimulation. Set pre-
319 stimulus membrane potentials were established by manual injection of bias currents of
320 appropriate amplitudes for the experiments. Current threshold was defined as the
321 minimum amount of current necessary to trigger an Action Potential (AP) and was
322 determined by injecting depolarizing 200 ms current steps in 5 pA increments until an
323 AP was triggered. In order to assess the firing properties, incremental depolarizing 500
324 ms current steps up to 500 pA were applied. The elicited APs were counted and plotted
325 against the current injection intensity. Recorded data were processed offline using
326 pClamp v10.6, Origin 2017 and Excel.

JNeurosci Accepted Manuscript

327 Unless otherwise stated, data are expressed as mean ± SEM. Analyses were
328 performed with SPSS24 and Origin 2017. Statistical tests used for each individual data
329 set and exact p-values are stated in the Results section.

330

331 **Results**

332 **Differences in pain in individuals carrying the same Na_V1.7-S241T mutation are**
333 **paralleled by differences in excitability of iPSC-SNs**

334 The clinical features of P300 and P301 were evaluated in two previous studies
335 (Geha et al., 2016; McDonnell et al., 2016). Despite carrying the same Nav1.7-S241T
336 mutation (**Figure 1A**), subjects P300 (son) and P301 (mother) reported very different
337 pain profiles (different number and duration of attacks, and number of awakening from
338 pain). In one study, P300 reported an average of 11.8 pain attacks per week while P301
339 reported 2.8 pain attacks per week. Mean duration of each pain attack for P300 was
340 378.3 min while for P301 it was 56.1 min (McDonnell et al., 2016). In the second study,
341 P300 reported time in pain of 424 minutes per day while P301 contemporaneously
342 reported 61 minutes; P300 reported average pain attack duration of 615 minutes while
343 P300 reported 91.5 minutes; and P300 reported 101 awakenings from pain over a 15
344 day period while P301 reported 1 awakening (Geha et al., 2016). Although variations in
345 pain profiles between individuals may reflect differences in processing at multiple levels
346 including higher CNS levels, we reasoned that differences in peripheral neurons might
347 also play a role, particularly in individuals with pain of peripheral origin, such as those
348 (e.g., P300 and P301) who carry a gain-of-function mutation in Na_V1.7 - a channel
349 which is mainly expressed in peripheral sensory neurons where it confers

JNeurosci Accepted Manuscript

350 hyperexcitability on them. To assess whether differences in pain profiles might be
351 modeled in an *in vitro* system containing only their peripheral neurons, we derived
352 iPSC-SNs from the affected son (P300) and mother (P301), as well as the unaffected
353 father (P303) using a differentiation protocol which produces pain-sensing sensory-like
354 neurons (Chambers et al., 2012; Cao et al., 2016; Chambers et al., 2016). The S241T
355 mutation was verified by Sanger sequencing in the iPSCs from P300 and P301 and
356 shown to be absent in P303. The iPSC-SNs stained positively for peripheral neuronal
357 marker (Peripherin), sensory neuronal marker (Brn3a), as well as Nav1.7 channel
358 (**Figure 1B**), and displayed neuronal morphology and electrophysiological properties
359 characteristic of mature neurons (**Figure 1C**). The expression of Nav1.7 was verified by
360 RT-PCR and shows that both P300 and P301 iPSC-SNs produce both wild-type and
361 S241T mutant transcripts, while samples from P303 produced only wild-type (WT)
362 transcripts (**Figure 1-1**).
363 We first studied the excitability of these iPSC-SNs using multi-electrode arrays
364 (MEA), a non-invasive, high-throughput, extracellular recording approach, that can
365 assess the excitability of intact neurons (Spira and Hai, 2013). MEA is capable of
366 accurately recording action potential (AP) firing of neurons as temperature is altered.
367 Because pain in individuals with IEM (including subjects P300 and P301) is triggered by
368 warmth, we assessed the firing of these intact iPSC-SNs at three different
369 temperatures: skin temperature (33°C), core body temperature (37°C), and nonnoxious
370 warmth (40°C). Neurons from both P300 and P301 displayed temperature-induced
371 increases in firing, as reflected by heat maps (**Figure 1D**). Elevating the temperature
372 increased both the mean firing frequency and number of neurons firing APs without

JNeurosci Accepted Manuscript

373 electrical stimulation, with neurons from P300 and P301, which carry the S241T
374 mutation, more excitable than these from P303, the unaffected father who does not
375 carry the mutation (**Figure 1D-F**). Indeed, we did not observe any firing from iPSC-SNs
376 derived from P303 at frequencies above 0.2 Hz, even at 40°C. Notably, while the
377 significant effect of the mutation on mean firing rate ($F = 24.7$, $p = 0.00002$; one-way
378 repeated measures ANOVA; 6 independent differentiations from 2 independent clones
379 for each line) and on number of active electrodes ($F = 192$, $p < 0.0001$; one-way
380 repeated measures ANOVA) was expected, we also observed significant differences in
381 excitability of iPSC-SNs between P300 and P301 (**Figure 1F**), who both carry the same
382 $Na_V1.7$-S241T mutation but reported differences in their pain. Compared to iPSC-SNs
383 from P301 (less pain), iPSC-SNs from P300 (more pain) displayed a significantly higher
384 firing frequency (33°C: P300 = 0.99 ± 0.16 Hz, P301 = 0.32 ± 0.07 Hz, $p = 0.01$; 37°C:
385 P300 = 1.56 ± 0.27 Hz, P301 = 0.51 ± 0.08 Hz; $p = 0.001$; 40°C: P300 = 2.1 ± 0.35 Hz,
386 P301 = 0.66 ± 0.09 Hz; $p = 0.001$; Bonferroni corrections) and significantly higher
387 number of active electrodes (33°C: P300 = 99 ± 5, P301 = 72 ± 5, $p = 0.01$, 37°C: P300
388 = 106 ± 5, P301 = 84 ± 3, $p = 0.001$, 40°C: P300 = 110 ± 4, P301 = 88 ± 3, $p = 0.0004$;
389 Bonferroni corrections), suggesting that for these individuals it might be possible to
390 model differences in pain profiles in an *in vitro* system of only subject-specific iPSC-
391 SNs.
392
393
394

JNeurosci Accepted Manuscript

395 **Subject-specific iPSC-SNs from P300 and P301 display differences in membrane**
396 **excitability that parallel differences in pain profiles**

397 A spectrum of differences in membrane properties might contribute to inter-
398 individual differences in activity of DRG neurons in different kindreds. To extend the
399 findings from the MEA assay to the level of membrane excitability in the family under
400 study, we used whole-cell patch-clamp for a head-to-head comparison of iPSC-SNs
401 from P300, P301 and P303, from differentiations prepared contemporaneously and
402 processed in parallel. These experiments revealed pronounced excitability differences
403 between iPSC-SNs from the three subjects. We assessed four major parameters that
404 reflect the levels of neuronal excitability: induced firing, percentage of neurons firing
405 repetitively, current threshold, and resting member potential (RMP). For all these four
406 parameters, we observed very clear and consistent differences in excitability between
407 iPSC-SNs from P300, P301 and P303 that again paralleled differences in pain profiles.
408 In response to graded suprathreshold 500 ms depolarizing stimuli, across the entire
409 current injection range, neurons derived from P300 fired the highest number of APs,
410 followed by neurons derived from P301, with P303 neurons firing at the lowest rate ($F =$
411 12, $p = 0.00006$, one-way ANOVA; Bonferroni corrections: P300 vs P301: $p = 0.037$;
412 P300 vs P303: $p = 0.00003$; P301 vs P303: $p = 0.044$; **Figure 2A-B**). When we
413 considered the percentage of multiple-spiking neurons, we observed a parallel set of
414 differences in excitability, with iPSC-SNs from P300 having the highest, and P303 the
415 lowest proportion of multiple-spiking (>1 AP) iPSC-SNs (**Figure 2C**).

416 iPSC-SNs from P300 were also found to have the lowest current threshold ($H =$
417 19.7, $p < 0.0005$, nonparametric ANOVA*;* Bonferroni corrections: P300 vs P301: $p =$

JNeurosci Accepted Manuscript

418 0.02, P300 vs P303 p = < 0.0005, P301 vs P303 p = 0.2). The data in **Figure 2D-E**
419 show that it is much harder to trigger an AP in neurons derived from P303 (unaffected
420 control), easier for P301 (less pain) and easiest for P300 (more pain), also consistent
421 with the pain reported by these individuals.

422 Interestingly, the RMP from these iPSC-SNs showed a similar pattern, with
423 membrane potential of P303 neurons most hyperpolarized, P300 neurons most
424 depolarized and P301 neurons in between (RMP: P300 = -54 ± 1 mV; P301 = -58 ± 1
425 mV and P303 = -61 ± 1 mV; F = 7, p = 0.002, one-way ANOVA; Bonferroni corrections:
426 P300 vs P301 p = 0.04, P300 vs P303 p = 0.002, P301 vs P303 p = 0.6; **Figure 2F**).
427

428 **Membrane potential contributes to the excitability difference observed between**
429 **iPSC-SNs**

430 It has been shown that in DRG neurons, neuronal excitability is dependent on
431 RMP (Harty et al., 2006; Huang et al., 2017). Following up on our observations of a
432 significant difference of 4 mV in RMP between iPSC-SNs from P301 and P300, in a
433 separate set of experiments we assessed the impact of membrane potential on
434 excitability of these neurons, again via a head-to-head comparison of iPSC-SNs from
435 paired differentiations prepared contemporaneously and processed in parallel. In these
436 experiments we studied the current threshold and firing rate of individual iPSC-SNs at
437 RMP before either depolarizing (P301) or hyperpolarizing (P300) the membrane
438 potential of each given neuron by 4 mV. We found that depolarizing neurons derived
439 from P301 by 4 mV resulted in a 25 ± 4% decrease in the current threshold, whereas
440 hyperpolarizing neurons derived from P300 caused a 24 ± 5% increase in current

JNeurosci Accepted Manuscript

441 threshold (**Figure 3A-B**). Consequently, there was not a significant difference in current
442 threshold between P300 and P301 when the difference in RMP was removed by
443 depolarizing neurons from P301 by 4 mV (**Figure 3C;** P300 = 35 ± 4 pA, n = 12; P301 =
444 36 ± 4 pA, n = 10; t = 0.1, p = 0.9, two-tailed unpaired t test) or by hyperpolarizing
445 neurons from P300 by 4 mV (**Figure 3D;** P300 = 51 ± 6 pA, n = 12; P301 = 45 ± 5 pA; t
446 = 0.1, p = 0.9, two-tailed unpaired t test). Similarly, using the same paradigm to study
447 the firing rate of both groups of iPSC-SNs, we found that there was no significant
448 difference in firing rate between iPSC-SNs derived from P300 and P301 when studied
449 at matched membrane potentials by hyperpolarizing iPSC-SNs from P300 by 4 mV
450 (**Figure 3E;** F = 0.9, p = 0.4; repeated measures one way ANOVA; n: P300 = 11, P301
451 = 10) or by depolarizing neurons from P301 by 4 mV (**Figure 3F;** F = 1.3, p = 0.3;
452 repeated measures one way ANOVA; n: P300 = 11, P301 = 10). These results indicate
453 that the difference in RMP between iPSC-SNs from P300 and P301 contributes to the
454 difference in excitability of these neurons.
455
456 **Whole exome sequencing (WES) reveals potential modifiers of sensory neuron**
457 **excitability**
458 Because subjects P300 (severe pain) and P301 (moderate pain) share the same
459 Na_V1.7-S241T mutation, we hypothesized that additional genetic variations might
460 contribute to the difference in excitability between iPSC-SNs from P300 and P301. To
461 identify these potential modifiers in the family under study, we performed WES on
462 samples from this family and filtered the resulting variants according to their expression
463 in DRG neurons using Ingenuity Pathway Analysis (IPA, Build 470319M Version

JNeurosci Accepted Manuscript

464 43605602), a manually-curated knowledge database created from the peer-reviewed
465 biomedical literature. WES confirmed the S241T mutation in both P300 and P301 but
466 not in the P303.

467 The WES analysis identified 90 variants in P300 and P301 in genes known to be
468 expressed in DRG neurons (9 in P300 and 81 in P301) (**Figure 4A; Figure 4-1**). Since
469 we found significant differences in excitability between iPSC-SNs from P300 and P301
470 (**Figure 2A-E**), we interrogated specific Gene Ontology processes and functions related
471 to neuronal excitability ('Excitation of neuron' and 'Neuronal Action Potential'). These
472 terms identified a variant in *KCNQ2*, the gene which encodes potassium channel Kv7.2,
473 in subject P301 (mother), but not in P300 (son; **Figure 4B**). Notably, Kv7.2 contributes
474 to the non-inactivating M current (I_M) (produced by Kv7.2, Kv7.3 and Kv7.5 channels in
475 DRG neurons), which has been shown to be a major determinant of the RMP of small-
476 diameter rat DRG neurons, where it regulates excitability (Passmore et al., 2003; Du et
477 al., 2014). Kv7.2 has also been found to be the main Kv7 channel isoform expressed in
478 rat DRG neurons (Rose et al., 2011). The identified heterozygous missense variant
479 c.2188A>G in exon 17 of the *KCNQ2* gene results in substitution of polar and
480 hydrophilic Threonine to non-polar and hydrophobic Alanine at p.730 in the C terminus
481 of the Kv7.2 channel (p.Thr730Ala; **Figure 4D, top panel**), has not been previously
482 reported, and is found exclusively in P301 (**Figure 4C**). After confirming the expression
483 of Kv7.2-WT in iPSC-SNs from P300, and the Kv7.2-T730A variant in P301 (**Figure 4D,**
484 **lower panel)**, we proceeded to validating the impact of this variant on the excitability of
485 iPSC-SNs from P301.

JNeurosci Accepted Manuscript

486 In order to establish whether the current produced by Kv7.2-T730A contributes to
487 excitability of iPSC-SNs derived from P301 by modulating I_M in these neurons, we
488 determined the effect of the mutation on I_M via perforated patch-clamp analysis. We
489 then used these data to investigate the influence of this variant on the excitability of
490 iPSC-SNs via dynamic-clamp (DC), an approach which combines the strategy of patch-
491 clamp and computer simulation methods (Prinz et al., 2004), permitting the current
492 produced by a mutant ion channel to be replaced with a precisely titrated amount of WT
493 current so that, in each cell studied, the effect of the mutant channel on excitability can
494 be assessed (Vasylyev et al., 2014).

495

496 **The T730A substitution in Kv7.2 causes a gain-of-function of I_M-current**

497 To characterize the I_M in iPSC-SNs from P300 and P301 in voltage-clamp we
498 used perforated-patch recordings. The current was activated by holding the membrane
499 at a steady depolarized potential (-20 mV) and then deactivated by hyperpolarizing
500 steps. Since I_M does not inactivate, this protocol minimizes potential contamination by
501 other voltage-gated currents (Adams and Brown, 1982). We inhibited Na^+ currents, fast-
502 activating Kv1 and Kv3-type K^+ current and HCN currents by including in the recording
503 solution their respective blockers: tetrodotoxin, 4-AP, and ZD-7288. Representative
504 traces of I_M recorded from iPSC-SNs from P300 and P301 are shown in **Figure 4E**. The
505 I-V curves and conductance, obtained using an established protocol (Adams and
506 Brown, 1982; Wang et al., 1998; Passmore et al., 2003), are shown in **Figure 4F**. There
507 was a 6 mV hyperpolarized shift in the $V_{1/2}$ of I_M conductance in neurons derived from
508 P301 (P300: $V_{1/2}$ = -60.9 ± 1.8 mV, n = 11; P301: $V_{1/2}$ = -67.3 ± 1.8 mV, n = 10; t = 2.6, p

JNeurosci Accepted Manuscript

509 = 0.02; two-tailed unpaired t-test). The hyperpolarizing shift is a gain-of-function
510 attribute, suggesting an enhancement in I_M around RMP.
511
512 **The Kv7.2-T730A variant hyperpolarizes resting membrane potential and reduces**
513 **excitability of iPSC-SNs**
514 To further establish the role of Kv7.2-T730A expression in modulating the
515 excitability of sensory neurons, we used dynamic clamp to subtract the current
516 produced by these mutant channels in iPSC-SNs from P301 and replace it with
517 precisely titrated injections of WT Kv7.2 current. To simulate I_M conductance at
518 physiologically relevant levels in iPSC-SNs, we constructed a model built from the
519 experimentally determined values of WT I_M current (obtained from P300 iPSC-SNs) and
520 mutant I_M current (obtained from P301 iPSC-SNs expressing the Kv7.2-T730A variant).
521 **Figure 5A** shows computer simulation of current traces and *n* activation gate from WT
522 I_M and Kv7.2-T730A I_M model. Steady-state current values from the I_M models show a
523 similar shift in normalized I-V relationship and voltage-dependence of activation (**Figure**
524 **5B**) as in the perforated patch recordings (**Figure 4F**). We obtained a value of 4 nS as
525 the maximum conductance - equivalent to the maximal current measured in the voltage-
526 clamp recordings (WT I_M: 220 ± 36 pA, n = 11; T730A I_M: 195 ± 25 pA, n = 10; t = 0.003,
527 p = 0.99, two-tailed unpaired t test). This is a very conservative estimate of the maximal
528 conductance, as voltage-dependence and kinetics of I_M in iPSC-SNs were examined
529 using the classical deactivation protocol with the final voltage step of -20 mV, to prevent
530 contamination by other voltage-dependent potassium currents (Shah et al., 2008). The
531 maximal opening of Kv7 channels is expected to occur at potentials more positive to -20

JNeurosci Accepted Manuscript

532 mV. Indeed, extrapolation of our experimental data suggests a maximum current close
533 to 400 pA (**Figure 5-1**), corresponding to ~8 nS maximum conductance. Hence, we
534 examined the contribution of Kv7.2-T730A I_M to changes in RMP and current threshold
535 in P301 iPSC-SNs, by substituting Kv7.2-T730A I_M, which we expect to be 50% of the
536 total current, with 50% WT I_M conductance, using dynamic clamp and implementing 4,
537 6, 8 and 10 nS maximum conductance levels. The effect of Kv7.2-T730A I_M on RMP
538 was measured, as shown in **Figure 5C**. Substituting the Kv7.2-T730A I_M with an
539 equivalent amount of WT conductance, caused RMP depolarization in an incremental
540 fashion with increasing amounts of overall conductance. The average values are
541 presented in **Figure 5D** and reveal depolarization of 2.2 ± 0.3 mV with 4 nS
542 conductance (t = 7, p = 0.001, two-tailed paired t-test, n = 9), 3.6 ± 0.6 mV with 6 nS
543 conductance (t = 6, p = 0.005, two-tailed paired t-test, n = 5), 4.6 ± 0.6 mV with 8 nS
544 conductance (t = 7, p = 0.002, two-tailed paired t-test, n = 5) and 6.4 ± 1 with 10 nS
545 conductance (t = 6, p = 0.004, two-tailed paired t-test, n = 5). Spontaneous firing was
546 observed in two additional iPSC-SNs at conductances greater than 4 nS (example trace
547 in **figure 5E**) and 6 nS (trace not shown).

548 We also assessed the effect of the Kv7.2-T730A variant on current threshold of
549 iPSC-SNs from P301. The reduction in current threshold from baseline (dynamic clamp
550 off) is presented in **Figure 5F** for individual iPSC-SNs (grey symbols) and the average
551 (blue symbols) for the same range of conductances of 4 - 10 nS. Substitution of 50%
552 Kv7.2-T730A I_M with 50% WT I_M with 4 nS maximal I_M conductance produced a
553 significant reduction in current threshold of 26 ± 3 % (p = 0.004, two-tailed paired t-test,
554 n = 8). Conductances of 6, 8 and 10 nS resulted in average threshold reductions of 39 ±

JNeurosci Accepted Manuscript

555 4 % (p = 0.005, two-tailed paired t-test, n = 6), 60 ± 9 % (p = 0.003, two-tailed paired t-
556 test, n = 6) and 63 ± 13 % (p = 0.01, two-tailed paired t-test, n = 5) respectively. One
557 cell became spontaneously active in response to substitution at 8 nS and one at 10 nS
558 (represented by a reduction of 100% in threshold in response to switching on the
559 dynamic clamp model). Taken together with the data from **Figure 5C-E**, these results
560 confirm that, in the family we studied, the T730A variant in Kv7.2 significantly reduces
561 the excitability of iPSC-SNs derived from subject P301 (less pain), even at the most
562 conservative estimate of maximal conductance of 4 nS.
563
564 **Discussion:**
565 Pain is universal but individual-to-individual differences are well documented.
566 Here we show, first, that at least in some cases, inter-individual differences in pain can
567 be modeled in a disease-in-a-dish model using subject-specific iPSC-SNs, second that
568 in some cases, mechanisms operating in peripheral sensory neurons can contribute to
569 inter-individual differences in pain, and third, we provide proof-of-concept that subject-
570 specific iPSCs and WES can be used to investigate peripheral mechanisms and
571 pinpoint specific gene variants that modulate pain signaling and contribute to inter-
572 individual differences in pain within a single family.
573 In this study, we demonstrate that a “pain-in-a-dish” *in vitro* disease model using
574 subject-specific iPSC-SNs parallels differences in pain, as reported by human subjects
575 included in this study. This iPSC-derived model revealed differences in current
576 threshold, firing frequency, responses to elevated temperature and number of
577 spontaneously active sensory neurons. Our results suggest that depolarized membrane

JNeurosci Accepted Manuscript

578 potential is a major factor responsible for the difference in excitability seen between
579 subjects P300 (more pain) and P301 (less pain) in the family under study. These data
580 demonstrate, for the first time, that in some cases inter-individual differences in chronic
581 pain can be modeled and studied *in vitro*. Using WES, we identified multiple candidate
582 genes (**Figure 4-1**) that may serve as modifiers of sensory neuron excitability in these
583 individuals. Building upon these observations we used Gene Ontology analysis to focus
584 on a variant in one gene, *KCNQ2*, as a candidate pain-modifier gene that might
585 contribute to inter-individual differences in pain in the family we studied, and
586 demonstrated by dynamic-clamp that a variant in *KCNQ2* reduces sensory neurons
587 excitability and thus is a contributor to pain resilience in the subject with less pain.
588 Inherited erythromelalgia (IEM), a severe pain syndrome characterized by
589 episodes of intense burning pain triggered by mild warmth, is caused by mutations in
590 sodium channel Nav1.7, which is preferentially expressed in peripheral sensory
591 neurons. Microneurographic recordings from IEM patients point to firing of C-fibers as a
592 cause of pain (Orstavik et al., 2003; Namer et al., 2015). Our previous studies indicate
593 that rodent DRG neurons expressing pathogenic human $Na_V1.7$ mutant channels from
594 patients with IEM are more excitable than DRG neurons expressing WT $Na_V1.7$
595 channels (Dib-Hajj et al., 2013), consistent with the notion that increased firing of DRG
596 neurons is associated with neuropathic pain (Ochoa and Torebjork, 1989; Kleggetveit et
597 al., 2012; Devor, 2013; Zhang et al., 2013; Haroutounian et al., 2014; Vaso et al., 2014).
598 Individual-to-individual variations in pain profiles have been well-documented in the
599 clinical domain, even within relatively homogenous patient groups, such as family
600 members with IEM due to the same Nav1.7 mutation (McDonnell et al., 2016). However,

JNeurosci Accepted Manuscript

601 these earlier studies have not provided any mechanistic insights regarding differences
602 in pain experience in different individuals.

603 In the present study we capitalized on differences in pain profiles in a unique
604 family containing two related IEM individuals (mother and son) carrying the same
605 Na_V1.7-S241T mutation (Geha et al., 2016; McDonnell et al., 2016). This mother/son
606 pair differed markedly in terms of overall time in pain, the duration of pain attacks, and
607 the number of awakenings due to pain. The mother and son pair carried the same
608 mutation, which is known to make the DRG neurons hyperexcitable (Yang et al., 2012),
609 but their distinct pain profiles presented an opportunity to study inter-individual
610 differences in pain within a single family, in an iPSC model. Given that Nav1.7 channels
611 are mainly expressed in the peripheral nervous system (Toledo-Aral et al., 1997; Dib-
612 Hajj et al., 2013), a fundamental question was whether neurons of the peripheral
613 nervous system could contribute to differences in pain without the inclusion of a CNS
614 component. In our “pain-in-a-dish” disease model, we confirmed that subject-specific
615 iPSC-SNs generated from family members carrying a Nav1.7 mutation are more
616 excitable than neurons derived from an unaffected family member. Using this “pain-in-a-
617 dish” disease model, we observed, for the first time, that an *in vitro* model with
618 peripheral sensory neurons alone, without a central component, can recapitulate the
619 difference in pain reported by different individuals. Although we acknowledge that CNS
620 components may still play an important role in the overall “pain experience”, and our
621 study cannot rule out the involvement of central processes in modulating the pain
622 experienced by our subjects, our data indicate that the difference in pain between these

JNeurosci Accepted Manuscript

623 individuals is at least partially due to the difference in excitability of their peripheral
624 neurons.
625 In the current study, we used WES to search for putative genetic modifiers that
626 might contribute to the difference in pain in these two clinically well-studied individuals.
627 Since the present study focused on the excitability of sensory neurons, we filtered the
628 obtained variants according to expression in DRG neurons. Our data revealed 90
629 genetic variations between mother and son, with 81 variants specific to the mother and
630 9 to the son. Further interrogation of those variants focused on their suggested role in
631 neuronal excitability and identified the Kv7.2-T730A variant in iPSC-SNs derived from
632 the mother as a potential modifier of sensory neuron excitability. The Kv7.2 channel is
633 known to regulate excitability of nociceptive DRG neurons (Passmore et al., 2003;
634 Young et al., 2014). Using dynamic clamp, we established that heterozygous
635 expression of this variant plays a significant role in downregulating the excitability of
636 iPSC-SNs derived from the mother, via a hyperpolarization of RMP and an increase in
637 current threshold, providing a genomic and mechanistic basis for the difference in pain
638 in these two individuals.
639 It is possible that additional gene variants, including variants with small effects,
640 may contribute to the differences we observed in excitability of iPSC-SNs derived from
641 the two subjects. We cannot rule out variations in genes not currently known to be
642 involved in neuronal excitability, which might indirectly influence peripheral neuron firing.
643 Further studies will be needed to assess the contributions of any variants of this type,
644 and to address whether epigenetic factors that influence sensory neuron firing or
645 differences in pain processing at higher levels in the CNS contribute to intrafamilial

variability. Importantly, we note that other gene variants might contribute to inter-individual differences in pain in other families. Nevertheless, our study provides proof-of-concept that subject-specific iPSCs and WES can be used to investigate peripheral mechanisms and pinpoint specific gene variants that modulate pain signaling and contribute to inter-individual differences in pain.

In summary, this study shows that an *in vitro* model of subject-specific iPSC-SNs from two related subjects can recapitulate aspects of individual-to-individual differences in pain, highlighting the value of studying iPSCs from individual subjects to create "disease-in-a-dish" models. Our results indicate that inter-individual differences in peripheral sensory neurons can, at least in some cases, contribute to differences in pain, and provide proof-of-principle that it is possible to pinpoint, within a single family, a specific gene that contributes to inter-individual differences in pain.

JNeurosci Accepted Manuscript

JNeurosci Accepted Manuscript

669 **References:**

670

671 Adams PR, Brown DA (1982) Synaptic inhibition of the M-current: slow excitatory post-
672 synaptic potential mechanism in bullfrog sympathetic neurones. J Physiol
673 332:263-272.
674 Adams PR, Brown DA, Constanti A (1982) M-currents and other potassium currents in
675 bullfrog sympathetic neurones. J Physiol 330:537-572.
676 Battefeld A, Tran BT, Gavrilis J, Cooper EC, Kole MH (2014) Heteromeric Kv7.2/7.3
677 channels differentially regulate action potential initiation and conduction in
678 neocortical myelinated axons. J Neurosci 34:3719-3732.
679 Cao L et al. (2016) Pharmacological reversal of a pain phenotype in iPSC-derived
680 sensory neurons and patients with inherited erythromelalgia. Sci Transl Med
681 8:335ra356.
682 Chambers SM, Mica Y, Lee G, Studer L, Tomishima MJ (2016) Dual-SMAD
683 Inhibition/WNT Activation-Based Methods to Induce Neural Crest and Derivatives
684 from Human Pluripotent Stem Cells. Methods in molecular biology 1307:329-343.
685 Chambers SM, Qi Y, Mica Y, Lee G, Zhang XJ, Niu L, Bilsland J, Cao L, Stevens E,
686 Whiting P, Shi SH, Studer L (2012) Combined small-molecule inhibition
687 accelerates developmental timing and converts human pluripotent stem cells into
688 nociceptors. Nat Biotechnol 30:715-720.
689 Devor M (2013) Neuropathic pain: pathophysiological response of nerves to injury. In:
690 Wall and Melzack's Textbook of Pain., 6th Edition (McMahon SL, Koltzenburg,
691 M., Tracey, I. and Turk, D.C. , ed), pp pp861-888. London: Churchill Livingstone.
692 Dib-Hajj SD, Yang Y, Black JA, Waxman SG (2013) The Na(V)1.7 sodium channel:
693 from molecule to man. Nat Rev Neurosci 14:49-62.
694 Drenth JP, Waxman SG (2007) Mutations in sodium-channel gene SCN9A cause a
695 spectrum of human genetic pain disorders. J Clin Invest 117:3603-3609.
696 Du X, Hao H, Gigout S, Huang D, Yang Y, Li L, Wang C, Sundt D, Jaffe DB, Zhang H,
697 Gamper N (2014) Control of somatic membrane potential in nociceptive neurons
698 and its implications for peripheral nociceptive transmission. Pain 155:2306-2322.
699 Geha P, Yang Y, Estacion M, Schulman BR, Tokuno H, Apkarian AV, Dib-Hajj SD,
700 Waxman SG (2016) Pharmacotherapy for Pain in a Family With Inherited
701 Erythromelalgia Guided by Genomic Analysis and Functional Profiling. JAMA
702 Neurol 73:659-667.
703 Haroutounian S, Nikolajsen L, Bendtsen TF, Finnerup NB, Kristensen AD, Hasselstrom
704 JB, Jensen TS (2014) Primary afferent input critical for maintaining spontaneous
705 pain in peripheral neuropathy. Pain 155:1272-1279.
706 Harty TP, Dib-Hajj SD, Tyrrell L, Blackman R, Hisama FM, Rose JB, Waxman SG
707 (2006) Na(V)1.7 mutant A863P in erythromelalgia: effects of altered activation
708 and steady-state inactivation on excitability of nociceptive dorsal root ganglion
709 neurons. J Neurosci 26:12566-12575.
710 Huang J, Vanoye CG, Cutts A, Goldberg YP, Dib-Hajj SD, Cohen CJ, Waxman SG,
711 George AL, Jr. (2017) Sodium channel NaV1.9 mutations associated with
712 insensitivity to pain dampen neuronal excitability. J Clin Invest 127:2805-2814.

JNeurosci Accepted Manuscript

713 Inoue H, Nagata N, Kurokawa H, Yamanaka S (2014) iPS cells: a game changer for
714 future medicine. The EMBO journal 33:409-417.
715 Jin SC et al. (2017) Contribution of rare inherited and de novo variants in 2,871
716 congenital heart disease probands. Nat Genet 49:1593-1601.
717 Kleggetveit IP, Namer B, Schmidt R, Helas T, Ruckel M, Orstavik K, Schmelz M, Jorum
718 E (2012) High spontaneous activity of C-nociceptors in painful polyneuropathy.
719 Pain 153:2040-2047.
720 Lampert A, Dib-Hajj SD, Tyrrell L, Waxman SG (2006) Size matters: Erythromelalgia
721 mutation S241T in Nav1.7 alters channel gating. J Biol Chem 281:36029-36035.
722 McDonnell A, Schulman B, Ali Z, Dib-Hajj SD, Brock F, Cobain S, Mainka T, Vollert J,
723 Tarabar S, Waxman SG (2016) Inherited erythromelalgia due to mutations in
724 SCN9A: natural history, clinical phenotype and somatosensory profile. Brain
725 139:1052-1065.
726 McNeish J, Gardner JP, Wainger BJ, Woolf CJ, Eggan K (2015) From Dish to Bedside:
727 Lessons Learned While Translating Findings from a Stem Cell Model of Disease
728 to a Clinical Trial. Cell Stem Cell 17:8-10.
729 Namer B, Orstavik K, Schmidt R, Kleggetveit IP, Weidner C, Mork C, Kvernebo MS,
730 Kvernebo K, Salter H, Carr TH, Segerdahl M, Quiding H, Waxman SG,
731 Handwerker HO, Torebjork HE, Jorum E, Schmelz M (2015) Specific changes in
732 conduction velocity recovery cycles of single nociceptors in a patient with
733 erythromelalgia with the I848T gain-of-function mutation of Nav1.7. Pain
734 156:1637-1646.
735 Ochoa J, Torebjork E (1989) Sensations evoked by intraneural microstimulation of C
736 nociceptor fibres in human skin nerves. J Physiol 415:583-599.
737 Orstavik K, Weidner C, Schmidt R, Schmelz M, Hilliges M, Jorum E, Handwerker H,
738 Torebjork E (2003) Pathological C-fibres in patients with a chronic painful
739 condition. Brain 126:567-578.
740 Passmore GM, Selyanko AA, Mistry M, Al-Qatari M, Marsh SJ, Matthews EA,
741 Dickenson AH, Brown TA, Burbidge SA, Main M, Brown DA (2003) KCNQ/M
742 currents in sensory neurons: significance for pain therapy. J Neurosci 23:7227-
743 7236.
744 Petrovic MM, Nowacki J, Olivo V, Tsaneva-Atanasova K, Randall AD, Mellor JR (2012)
745 Inhibition of post-synaptic Kv7/KCNQ/M channels facilitates long-term
746 potentiation in the hippocampus. PLoS One 7:e30402.
747 Prinz AA, Abbott LF, Marder E (2004) The dynamic clamp comes of age. Trends
748 Neurosci 27:218-224.
749 Rose K, Ooi L, Dalle C, Robertson B, Wood IC, Gamper N (2011) Transcriptional
750 repression of the M channel subunit Kv7.2 in chronic nerve injury. Pain 152:742-
751 754.
752 Shah MM, Migliore M, Valencia I, Cooper EC, Brown DA (2008) Functional significance
753 of axonal Kv7 channels in hippocampal pyramidal neurons. Proc Natl Acad Sci U
754 S A 105:7869-7874.
755 Soliman MA, Aboharb F, Zeltner N, Studer L (2017) Pluripotent stem cells in
756 neuropsychiatric disorders. Mol Psychiatry.
757 Spira ME, Hai A (2013) Multi-electrode array technologies for neuroscience and
758 cardiology. Nature nanotechnology 8:83-94.

JNeurosci Accepted Manuscript

759 Toledo-Aral JJ, Moss BL, He ZJ, Koszowski AG, Whisenand T, Levinson SR, Wolf JJ,
760 Silos-Santiago I, Halegoua S, Mandel G (1997) Identification of PN1, a
761 predominant voltage-dependent sodium channel expressed principally in
762 peripheral neurons. Proc Natl Acad Sci U S A 94:1527-1532.
763 Vaso A, Adahan HM, Gjika A, Zahaj S, Zhurda T, Vyshka G, Devor M (2014) Peripheral
764 nervous system origin of phantom limb pain. Pain 155:1384-1391.
765 Vasylyev DV, Han C, Zhao P, Dib-Hajj S, Waxman SG (2014) Dynamic-clamp analysis
766 of wild-type human Nav1.7 and erythromelalgia mutant channel L858H. J
767 Neurophysiol 111:1429-1443.
768 Wang HS, Pan Z, Shi W, Brown BS, Wymore RS, Cohen IS, Dixon JE, McKinnon D
769 (1998) KCNQ2 and KCNQ3 potassium channel subunits: molecular correlates of
770 the M-channel. Science 282:1890-1893.
771 Yang Y, Adi T, Effraim PR, Chen L, Dib-Hajj SD, Waxman SG (2017) Reverse
772 pharmacogenomics: carbamazepine normalizes activation and attenuates
773 thermal hyperexcitability of sensory neurons due to Nav 1.7 mutation I234T. Br J
774 Pharmacol.
775 Yang Y, Dib-Hajj SD, Zhang J, Zhang Y, Tyrrell L, Estacion M, Waxman SG (2012)
776 Structural modelling and mutant cycle analysis predict pharmacoresponsiveness
777 of a Na(V)1.7 mutant channel. Nat Commun 3:1186.
778 Yang Y, Huang J, Mis MA, Estacion M, Macala L, Shah P, Schulman BR, Horton DB,
779 Dib-Hajj SD, Waxman SG (2016) Nav1.7-A1632G Mutation from a Family with
780 Inherited Erythromelalgia: Enhanced Firing of Dorsal Root Ganglia Neurons
781 Evoked by Thermal Stimuli. J Neurosci 36:7511-7522.
782 Young GT, Gutteridge A, Fox H, Wilbrey AL, Cao L, Cho LT, Brown AR, Benn CL,
783 Kammonen LR, Friedman JH, Bictash M, Whiting P, Bilsland JG, Stevens EB
784 (2014) Characterizing human stem cell-derived sensory neurons at the single-cell
785 level reveals their ion channel expression and utility in pain research. Mol Ther
786 22:1530-1543.
787 Zaidi S et al. (2013) De novo mutations in histone-modifying genes in congenital heart
788 disease. Nature 498:220-223.
789 Zeltner N, Studer L (2015) Pluripotent stem cell-based disease modeling: current
790 hurdles and future promise. Curr Opin Cell Biol 37:102-110.
791 Zhang XY, Wen J, Yang W, Wang C, Gao L, Zheng LH, Wang T, Ran K, Li Y, Li X, Xu
792 M, Luo J, Feng S, Ma X, Ma H, Chai Z, Zhou Z, Yao J, Zhang X, Liu JY (2013)
793 Gain-of-function mutations in SCN11A cause familial episodic pain. Am J Hum
794 Genet 93:957-966.
795
796
797
798
799
800
801

JNeurosci Accepted Manuscript

802 **Figure legends**

803

804 **Figure 1. MEA recordings reveal differences in excitability between iPSC-SNs**
805 **from subjects carrying the Nav1.7-S241T mutation and an unaffected control.**

806 **(A)** Affected subjects P301 (mother) and P300 (son) carry the Nav1.7-S241T mutation,
807 whereas P303 (unaffected father) carries only wild-type alleles. **(B)** iPSC-SNs from
808 P300, P301 and P303 express canonical sensory neuron markers and Nav1.7. **Left**
809 **panel**: Peripherin (red), Brn3a (green), Islet1 (grey). **Figure 1-1** shows that the Nav1.7-
810 S241T mutation is present in iPSC-SNs from P300 and P301, but not P303. **Right**
811 **panel:** Peripherin (red), Nav1.7 (green), Pan Neuronal Marker (grey). **(C)** iPSC-SNs
812 from all three subjects showed a neuronal morphology (microphotograph, scale bar = 20
813 μm), produce large sodium and potassium currents and fire action potentials (APs)
814 (examples from P301 (middle panel) and P300 (right panel)). **(D)** MEA recordings of AP
815 firing of iPSC-SNs from P300, P301 and 303. Heatmaps show representative MEA
816 recordings. The firing frequency of each active electrode is color-coded: white/red - high
817 firing frequency; blue/black - low firing frequency. Each circle represents an active
818 electrode within an 8X8 electrode array. **Top panels*:*** recordings from iPSC-SNs from
819 P300 at 33°C, 37°C, 40°C. **Middle panels*:*** recordings from iPSC-SNs from P301 at
820 33°C, 37°C, 40°C. **Bottom panels**: recordings from iPSC-SNs from P303 at 33°C,
821 37°C, 40°C. **(E)** Representative MEA recordings showing neuronal firing at 33°C. **(F)**
822 **Top panel:** Average firing frequencies of neurons from P300, P301 and P303. **Bottom**
823 **panel:** Average numbers of active electrodes for P300, P301 and P303 (average of
824 three wells).

825

JNeurosci Accepted Manuscript

826 **Figure 2. Passive and firing properties of iPSC-SNs at RMP show differences in**
827 **excitability between P300, P301 and P303.**

828 **(A)** Input-output relationships for iPSC-SNs from P300 (orange), P301 (blue) and P303
829 (grey) subjects. Data are mean ± SEM. N: P300 = 18, P301 = 19, P303 = 15; F = 12, p
830 = 0.00006, one-way ANOVA; Bonferroni corrections: P300-P301 = 0.037, P300-P303 =
831 0.00003, P301-P303 = 0.044. **(B)** Example traces showing AP firing in iPSC-SNs from
832 P300, P301 and P303 in response to 500 ms 300 pA steps. **(C)** Charts showing the
833 percentage of single-spiking iPSC-SNs (P300: 12%; P301: 32%; P303: 87%). **(D)**
834 Current threshold values. Each symbol refers to an individual neuron; to the right are
835 mean (diamond symbol), median (line), SE (box) and confidence intervals (whiskers). N:
836 P300 = 16, P301 = 17, P303 = 12; $H = 19.7$, $p < 0.0005$, nonparametric ANOVA;
837 Bonferroni corrections: P300-P301 = 0.02, P300-P303 < 0.0005, P301-P303 = 0.2. **(E)**
838 Example traces showing the difference in current threshold between iPSC-SNs from
839 P300, P301 and P303. **(F)** RMP values for the three subjects. Each symbol refers to an
840 individual neuron. To the right are mean (diamond symbol), median (line), SE (box) and
841 confidence intervals (whiskers). N: P300 = 18, P301 = 19, P303 = 15; F = 7, p = 0.002,
842 one-way ANOVA; Bonferroni corrections: P300-P301 = 0.04, P300-P303 = 0.002, P301-
843 P303 = 0.6.

844 **Figure 3. Firing properties of iPSC-SNs from subjects P300 and P301 are not**
845 **significantly different at matched membrane potentials.**

846 **(A)** Graph showing the % change in current threshold after depolarizing (P301, n = 10,
847 blue) or hyperpolarizing (P300, n = 12, orange) the RMP of iPSC-SNs by 4 mV. **(B)**
848 Example recordings from neurons derived from P300 (orange) and P301 (blue) showing

JNeurosci Accepted Manuscript

849 the change in current threshold after either depolarizing (P301) or hyperpolarizing
850 (P300) the RMP of iPSC-SNs by 4 mV (the average difference in RMP between P300
851 and P301). **(C)** Scatter plot showing individual current threshold values for iPSC-SNs
852 from P300 (orange) at RMP, and P301 (blue) depolarized by 4 mV. **(D)** Scatter plot
853 showing individual current threshold values for iPSC-SNs from P301 (blue) at RMP and
854 P300 (orange) hyperpolarized by 4 mV. **(E) I**nput-output relationships for iPSC-SNs
855 from P300 and P301 at matched membrane potentials (obtained by hyperpolarizing
856 P300 neurons by 4 mV). **(F) I**nput-output relationships for iPSC-SNs at matched
857 membrane potentials (obtained by depolarizing P301 neurons by 4 mV). **(G)** Example
858 recordings from a neuron derived from P300 (orange) and P301 (blue) showing the
859 change in firing frequency after either depolarizing (P301) or hyperpolarizing (P300) the
860 RMP by 4 mV.

861 **Figure 4. Whole exome sequencing reveals a variant in KCNQ2 gene as a**
862 **potential modulator of neuronal excitability in iPSC-SNs from P301.**

863 **(A)** Venn diagram showing the numbers of detected variants in samples from P300,
864 P301 and P303. Full list of gene variants is included in extended **Figure 4-1**. **(B)**
865 Targeted Gene Ontology analysis directed towards neuronal excitability indicated
866 *KCNQ2* as a potential excitability modulator in P301. **(C)** The *KCNQ2* variant is present
867 in genome of P301 (mother), but not P300 (son) or P303 (father). **(D) Top panel:**
868 Location of the T730A mutation in the Kv7.2 channel. Boxes in the C-terminus indicate
869 the four α-helical regions (A, B, C and D) and the Ankyrin-G binding domain. **Lower**
870 **panel:** Kv7.2 is expressed in P300 and P301; agarose gel electrophoresis showing the
871 amplification of the expected product (512 bp) from cDNA samples of iPSC-SNs (the M

JNeurosci Accepted Manuscript

872 lane shows the100 bp molecular weight marker), and chromatogram of the sequence of
873 the obtained products showing only the Kv7.2-WT allele (ACC) in P300, and both
874 Kv7.2-WT and Kv7.2-T730A (GCC) allele in P301. **(E)** Representative perforated patch-
875 clamp recordings of I_M-current from P300 (orange) and P301 (blue) neurons; currents
876 evoked by a series of 1 s, 10 mV hyperpolarizing voltage steps from a holding potential
877 of -20 mV. **(F) Left panel:** Normalized current-voltage (I-V) curves for I_M -current
878 recorded from P300 and P301. **Right panel**: Comparison of voltage-dependence of
879 activation of I_M between P300 and P301 iPSCs-SNs. Data were corrected for LJP
880 (+8.2mV).

881 **Figure 5. Dynamic-clamp recordings confirm that Kv7.2-T730A I_M reduces the**
882 **excitability of iPSC-SNs derived from P301.**

883 (A) Current traces obtained from Kv7.2-WT I_M and Kv7.2-T730A I_M current model.
884 Currents were evoked from -110 to -20 mV from a holding potential of -20 mV. Time
885 sequence of *n* variable obtained in the model (lower panels) in response to a series of
886 voltage steps ranging from -110 to -20 mV. **(B) Left panel**: Comparison of steady-state
887 activation of the kinetic model of Kv7.2-WT I_M (orange) and Kv7.2-T730A I_M (blue).
888 **Right panel**: Normalized I-V relationship from P300 (Kv7.2-WT I_M; orange) and P301
889 (Kv7.2-T730A I_M; blue) models. **(C)** An example membrane potential response of a
890 P301 neuron to substituting the T730A I_M with WT I_M (-50% T730A I_M, +50% WT I_M) at
891 increasing amounts of conductance, based on the values from extrapolated data of the
892 maximum I_M current in iPSC-SNs in **Figure 5-1**. DC - dynamic clamp. **(D)** Average
893 response of P301 iPSC-SNs to the protocol from fig. 5C (n = 5 to 8). **(E)** Example trace
894 showing spontaneous firing of a P301 iPSC-SN in response to the protocol from fig. 5C.

JNeurosci Accepted Manuscript

895 **(F)** Substituting the T730A I_M current with WT I_M (-50% T730A I_M, +50% WT I_M) at
896 increasing amounts of conductance in P301 neurons results in significant reduction in
897 current threshold. Insets show responses of a representative neuron at each
898 conductance.

899
900
901 **Extended data legends:**
902
903 **Figure 1-1. Nav1.7-S241T mutation is expressed in iPSC-SNs from the affected**
904 **son (P300) and mother (P301), but not the unaffected father (P303).**

905 Agarose gel electrophoresis showing the amplification of the expected product (514 bp)
906 from cDNA samples of iPSC-SNs (the M lane shows the 100 bp molecular weight
907 marker) and chromatogram of the sequence of the obtained products confirms the
908 expression of both WT (TCA) and mutant (ACA) alleles in the samples from P300 and
909 P301, and only the WT allele in the sample from P303.

910

911 **Figure 4-1. The Whole Exome Sequencing analysis identified variants in P300,**
912 **P301, and P303 in genes known to be expressed in DRG neurons.**

913 P300 – gene variants identified in subject P300 (145). P301 – gene variants identified in
914 subject P301 (184), P303 – gene variants identified in subject P303 (175). P300_unique
915 – gene variants specific to subject P300 (9), P301_unique – gene variants specific to
916 subject P301 (81), P303_unique – gene variants specific to subject P303 (105).

917 **Figure 5-1. Extrapolation of the maximum I_M from iPSC-SNs derived from P300**
918 **and P301.**

919 The activation curve of I_M obtained from the experimental data was fit to Boltzmann
920 equation to find the peak current of 390 pA and $V_{½}$ of -30 mV for KCNQ2-T730A I_M
921 (P301) and -25mV for WT I_M (P300).

922

923

JNeurosci Accepted Manuscript

JNeurosci Accepted Manuscript

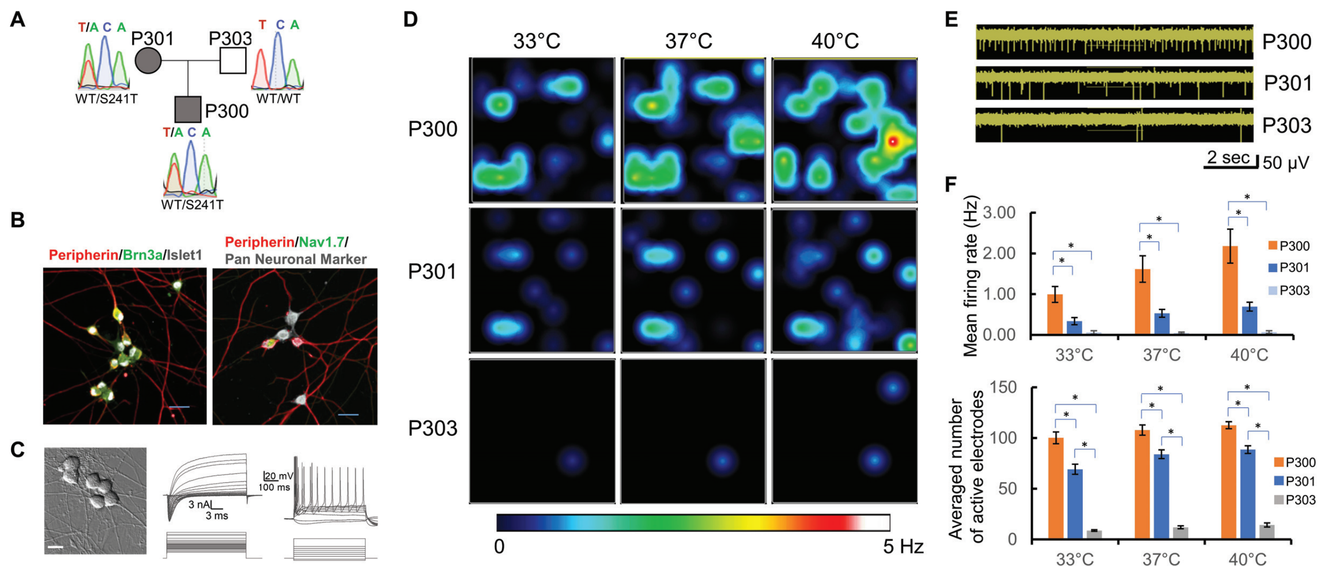

JNeurosci Accepted Manuscript

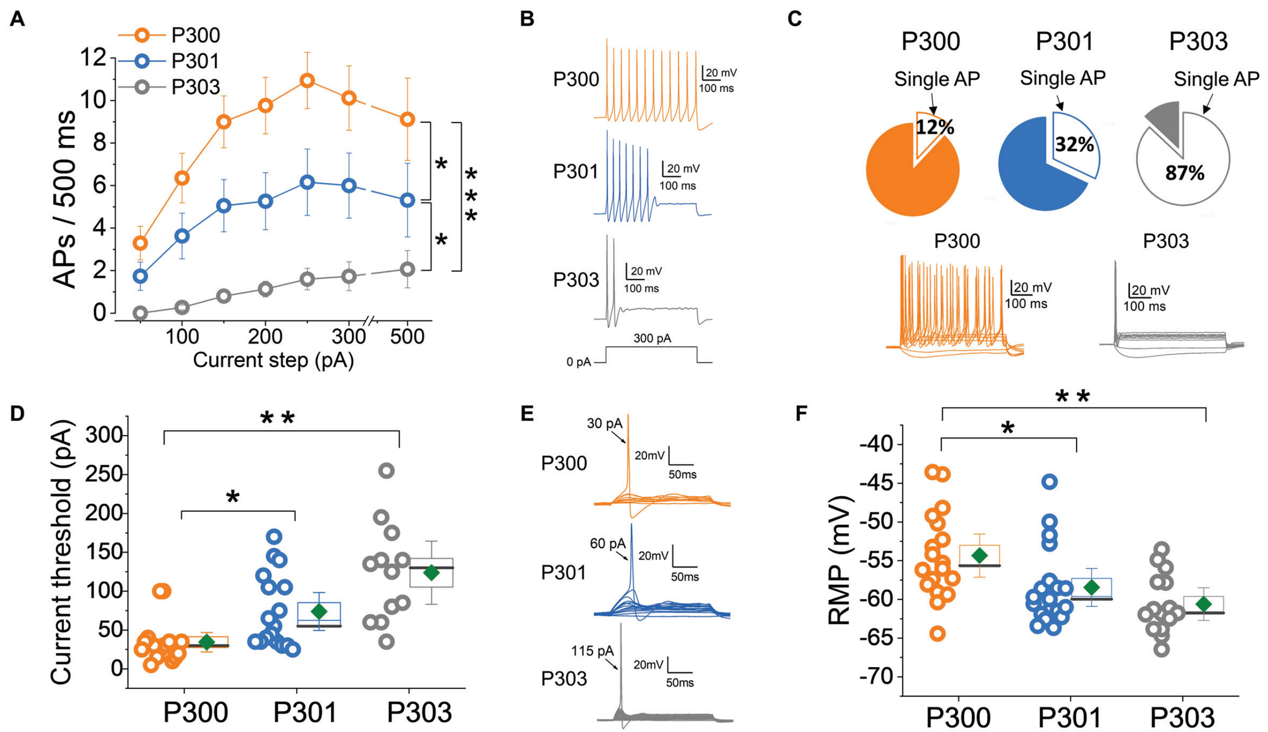

JNeurosci Accepted Manuscript

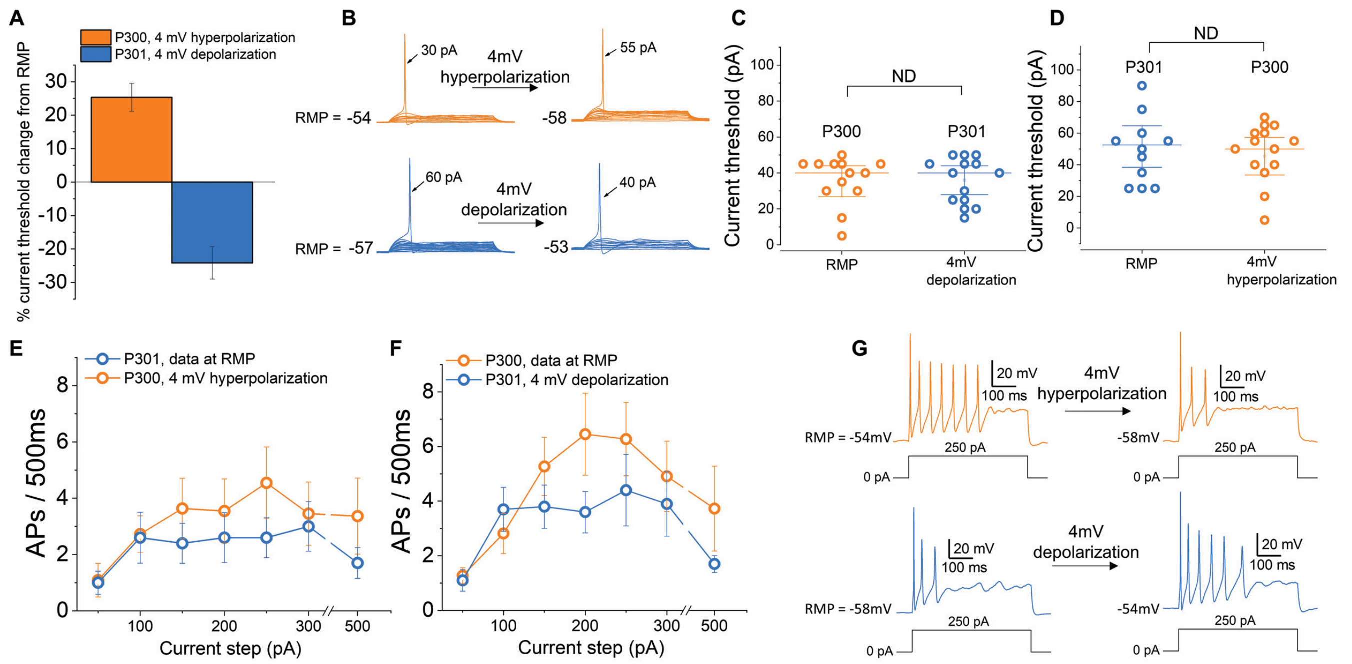

JNeurosci Accepted Manuscript

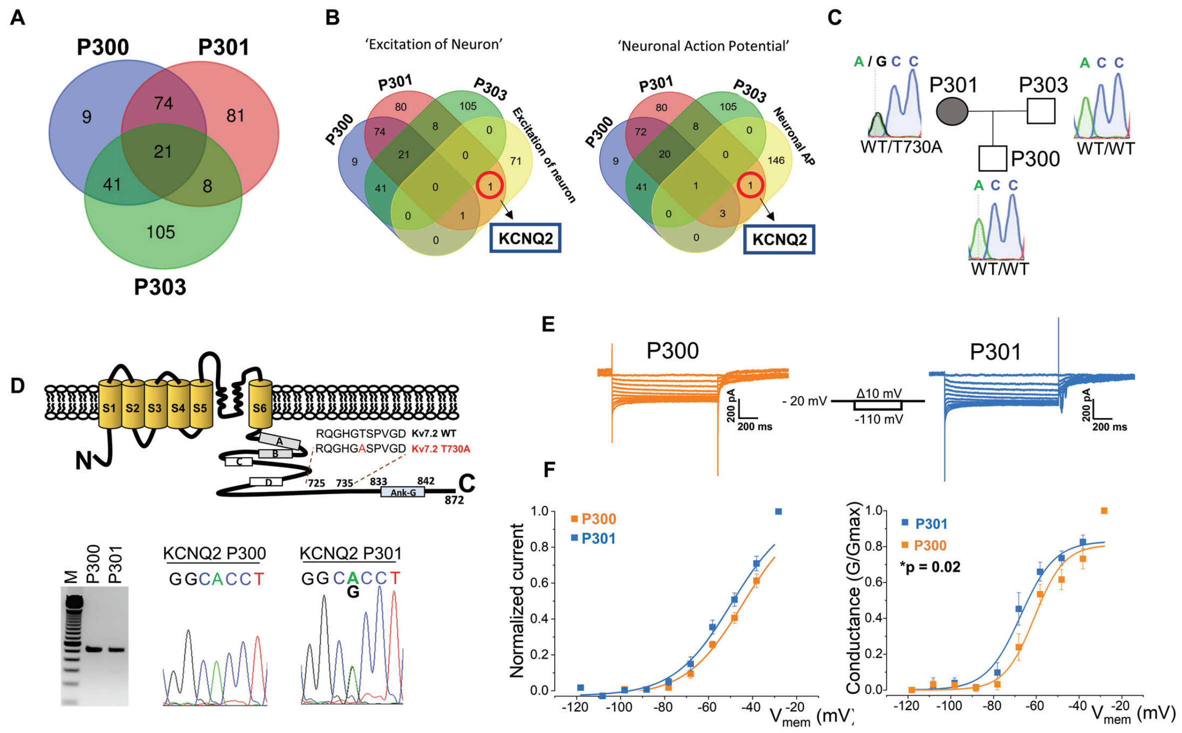

JNeurosci Accepted Manuscript